

Interfacial strength cross-over across silica- and graphite-cis-1,4-polyisoprene interfaces

Jeeno Jose, and Narasimhan Swaminathan

Citation: *Journal of Applied Physics* **123**, 245306 (2018); doi: 10.1063/1.5020776

View online: <https://doi.org/10.1063/1.5020776>

View Table of Contents: <http://aip.scitation.org/toc/jap/123/24>

Published by the *American Institute of Physics*

Articles you may be interested in

[Carrier scattering mechanisms limiting mobility in hydrogen-doped indium oxide](#)

Journal of Applied Physics **123**, 245102 (2018); 10.1063/1.5033561

[Structural and electronic properties of a-edge dislocations along \$\langle 1-100 \rangle\$ in GaN](#)

Journal of Applied Physics **123**, 244301 (2018); 10.1063/1.5034198

[3D simulation of superconducting magnetic shields and lenses using the fast Fourier transform](#)

Journal of Applied Physics **123**, 233901 (2018); 10.1063/1.5027592

[Integration of external electric fields in molecular dynamics simulation models for resistive switching devices](#)

Journal of Applied Physics **123**, 245301 (2018); 10.1063/1.5029877

[Carbide-derived carbons for dense and tunable 3D graphene networks](#)

Applied Physics Letters **112**, 251907 (2018); 10.1063/1.5030136

[Enhanced nonlinear optical susceptibilities in phosphorene nanoribbons: Ab initio study](#)

Journal of Applied Physics **123**, 245113 (2018); 10.1063/1.5029547

AIP | Journal of Applied Physics

SPECIAL TOPICS



Interfacial strength cross-over across silica- and graphite-*cis*-1,4-polyisoprene interfaces

Jeeno Jose and Narasimhan Swaminathan^{a)}

Department of Mechanical Engineering, Indian Institute of Technology Madras, Chennai 600 036, India

(Received 27 December 2017; accepted 23 May 2018; published online 27 June 2018)

A cross-over in the interfacial strength, with increase in the separation rate, is observed between graphite-*cis*-1,4-polyisoprene and amorphous silica-*cis*-1,4-polyisoprene interfaces. Molecular dynamics simulations are used to compare the traction-separation characteristics of the two interfaces in the opening mode of separation at various separation rates and temperatures above the glass transition temperature of *cis*-1,4-polyisoprene. It was observed that various parameters governing the interface strength, such as strength modulus (ratio of peak traction to the separation at peak traction), peak traction, and the work of adhesion are higher for the silica substrated interface at very low separation rates. However, at higher rates, the graphite substrated interface showed higher values for the strength parameters. The reasons for this interface strength cross-over are explained using the potential energy, mobility, entanglement strength, tensile stiffness, and densities of the polymer over both substrates and the interface cohesive binding energy. Based on these observations, it is concluded that silica filled rubber nanocomposites are suitable for normal automobile tire applications; however, graphite fillers may be more suitable for resisting very large impact loads. *Published by AIP Publishing.* <https://doi.org/10.1063/1.5020776>

I. INTRODUCTION

The use of rubber nanocomposites with low rolling resistance in automobile tire treads can lead to a significant reduction in green house gas emissions^{1,2} and increased fuel efficiencies. The nanocomposite material used to make tires consists of a rubber matrix and reinforcing fillers. The rubber matrix is usually *cis*-1,4-polyisoprene (PI), styrene-butadiene copolymer or polybutadiene. Two major fillers employed in tires are carbon black and silica. Of the two materials, silica is known to impart a better rolling resistance to tires.^{3,4} Although nano-fillers like carbon nanotubes (CNTs) and graphene layers have been recently explored for better reinforcement, carbon black and silica continue to be the major filler materials used in the tire industry.^{1,5,6}

One way to reduce the rolling resistance is to enhance the extent of mechanical reinforcement. This enhancement could be realized by attaining a better dispersion of fillers within the rubber matrix. Filler-rubber interactions play an important role in the dispersion of fillers. It is observed that the dispersion increases with the filler-rubber interfacial strength.⁶⁻⁸ A direct indicator of mechanical strength of the interface is the traction-separation ($\tau - \delta$) characteristics⁹⁻¹¹ which are generally obtained by interface cohesive zone separation in a direction normal to the interface (opening mode of separation).

Several factors and phenomena can affect the behavior of the interface and its strength. Atomistic level resolution of the interface is often required in order to understand the effect of these factors using experimental means, which is difficult to obtain even with the most sophisticated instruments.¹² Molecular simulations [e.g., Molecular Dynamics

(MD) technique] can resolve atomistic level details and shed insights into the cohesive zone separation at the nano-interfaces. A few research studies have explored the mechanical behavior of filler-polymer interfaces through the opening mode of interface separation^{9,11,13-20} and they have revealed several factors that alter interfacial strength. Many of these simulations use carbon based materials such as graphene, graphite or CNT as the filler material and it is instructive to examine how various aspects of the polymer or the filler affect the interface strength. In Refs. 9 and 13, the $\tau - \delta$ characteristics of the interface formed by graphene with amorphous glassy polyethylene (PE) were obtained. It was observed that the interface strength increases with the density of graphene functionalization.¹³ Large graphene aspect ratios enhanced the cohesive forces at graphene-cellulose¹⁵ and graphene-epoxy resin¹⁴ interfaces, where matrix polymers in both cases were in the amorphous glassy state. The cohesive force was increased by ~ 500 times when the interface was bridged using an ethylene molecule.¹⁴ Using MD simulations of generic filler-polymer interface configurations, it was shown that there exists an optimum degree of crosslinking of the polymer matrix which maximizes the interface cohesive binding,¹⁶ while lower inter-chain non-bonding interactions favored higher interface cohesive binding.¹⁷ Simulations of graphene/CNT/PE (amorphous glassy) hybrid interfaces conducted by Zhang *et al.*¹¹ reveal that the actual configuration of the interface can also affect its strength. Specifically, it was shown that the peak traction was slightly higher when the polymer was placed between two graphene layers, when compared to the configuration containing only one graphene layer. The influence of the CNT position with respect to the graphene layer and CNT diameter, on the location at which the interface completely separates (fractures) and on the peak traction experienced at

^{a)}n.swaminathan@iitm.ac.in

the graphene layer, were studied in Ref. 11. The type of the carbon based substrate or the polymer used also affects the interface strength. For example, Ref. 18 compared the opening mode behavior of the carbon nanofiber and graphite nanoplatelet substrates with an amorphous glassy PE matrix. The graphite nanoplatelet substrated interface had a higher peak traction and hence a higher strength. In another work, the polymer was changed and the interfaces were formed by graphene (either pristine graphene or graphene functionalized with -COOH) with PE (above glass transition temperature - T_g), polyurethane (above T_g), and polystyrene (below T_g). The interface opening was conducted at two different separation rates. The strength of each interface having specified functionalization and separating at the specified rate was compared with the strength of the bulk polymer undergoing uniaxial tension with the equivalent strain rate. These simulations revealed that, the failure need not always occur at the interface between the filler and the polymer. The ratio of the interface strength to the bulk polymer strength determined the position of the fracture, thereby indicating whether the interface is strong or weak.¹⁹ Similarly, simulations involving the interface opening of graphite-polyvinylidene difluoride (PVDF) were conducted to understand the mechanical failure in Li-ion batteries. The failure of the interface (rather than the polymer) was observed indicating that the interface strength was lower than the strength of the bulk PVDF or graphite.¹⁰ In a recent work,²⁰ the interface failure between graphene and *cis*-1,4-PI (above T_g) was studied at various temperatures and separation rates. The underlying interface deformation physics was explained based on the development of voids in the interface and chain straightening. It was observed that the separation rate has a significant effect on the traction response and the manner at which the interface deformed.²⁰

While the above-mentioned studies have shed significant insights into various factors affecting the interface strength by simulating interface opening for several combinations of fillers and polymers, the opening mode of separation for the silica-*cis*-1,4-PI interface has not been conducted till date. In this work, we compare the opening mode $\tau - \delta$ characteristics of the graphite-*cis*-1,4-PI interface and silica-*cis*-1,4-PI interface at various rates and temperatures using MD. The cohesive zone separation physics discussed in Ref. 20 pertaining to the polymer network deformations is explored in both the graphite substrated interface (GSI) and silica substrated interface (SSI) in order to understand the effect of carbon black and silica fillers, respectively, on interface interaction. In this paper, the term ‘‘cohesive energy’’ is used to denote the binding energy of the polymer and substrate at the interface, although this term is generally used to represent the energy which binds similar materials. We have chosen the *cis*-1,4-PI polymer since it is the principal part of the natural rubber.

II. MOLECULAR MODEL

A. Graphite model

In order to model graphite, the orthorhombic Fmmm unit cells²¹ of graphite were used. Graphite with 6 layers of graphene was used to model carbon black.²² The interactions

within the graphite substrate were modeled using the adaptive intermolecular reactive bond order (AIREBO) potential²³ with zero partial charge for the carbon atoms.

B. Silica model

To create the silica substrate, the cristobalite polymorph of silica belonging to the $P2_13$ space group with lattice parameter, $a = 7.16 \text{ \AA}$ (Ref. 24) was amorphized to produce a sample whose radial distribution functions $g_{\text{Si-Si}}(r)$, $g_{\text{O-O}}(r)$ and $g_{\text{Si-O}}(r)$ are in close agreement with the literature.²⁵ The bulk amorphous silica was prepared according to the procedure discussed in Refs. 25 and 26. The simulation box used was cubic and contained 8000 SiO_2 units. A combination of Coulomb and Buckingham terms $[V_{ij} = \frac{q_i q_j}{r} + A_{ij} \exp(-\frac{r}{\rho_{ij}}) - \frac{C}{r^6}]$ was used to model interaction within silica. The parameters for this potential are tabulated in Table I. The partial charges of silicon (Si) and oxygen (O) atoms in silica are $2.4e$ and $-1.2e$, respectively, with e being the electronic charge.²⁷ The lattice vectors were modified to obtain the density of vitreous silica at room temperature ($= 2.2 \text{ g/cm}^3$).²⁵ The system was then equilibrated in canonical [NVT - fixed number of particles (N), a fixed volume (V) and a fixed temperature (T)] ensemble at 4000 K for 0.4 ns and then annealed from 4000 K to 300 K at a rate of 2 K/ps before it was equilibrated again at 300 K for 0.4 ns. The cohesive energy per SiO_2 unit of the amorphous sample was -5335.48 kJ/mol and that of the crystalline silica was -5343.89 kJ/mol . Furthermore, the Buckingham interaction between Si atoms was neglected (Table I) as the distance between Si atoms is larger when compared to O-O and Si-O distances. The cohesive energy of cristobalite differed only by 4.27 kJ/mol when computed with and without Si-Si interaction (-5348.16 and -5343.89 kJ/mol , respectively).

In order to verify the values of the cohesive energy, we compared our values with the literature. The literature reports -5122.05 kJ/mol ²⁵ and -5151.34 kJ/mol ²⁸ for glass and cristobalite, respectively. These values are higher than the values obtained in this work since slightly different Buckingham potential parameters are used here. The parameters used in this work are more recent and are optimized to model silica surfaces,²⁷ while the parameterizations in Refs. 25 and 28 are used to model bulk samples of silica.

C. Polymer model

The united atom model as in Ref. 20 is used here. The carbon atom and attached hydrogen atoms, if any, were treated as a single lumped particle which will be termed as an ‘‘atom’’ from now on. The polymer network creation process was based on the SuSi algorithm which employs self-avoiding random walks to generate an energetically stable structure

TABLE I. Potential parameters for silica.²⁷

$i-j$	A_{ij} (kJ/mol)	ρ_{ij} (Å)	C_{ij} (kJ · Å ⁶ /mol)
Si-Si	0	1	0
Si-O	1321245.2700	0.1938	5272.3864
O-O	177871.8937	0.3436	18568.7204

TABLE II. Parameters for vdW interactions due to silica and graphite atoms.

Type, i	ϵ_i (kJ/mol)	σ_i (Å)
C ⁹	0.6192	3.6170
Si ²⁶	1.2552	3.1182
O ²⁶	0.6276	3.8264

with least torsional strains at single bonds.²⁹ The details of the exact parameters used in the network creation and the interatomic potential used to model *cis*-1,4-PI are mentioned in Ref. 20. The partial charge on each atom is zero. Bonds are permanent since there is no significant bond stretching during the separation of interface at any separation rate.²⁰ We employed a large cut-off of 22.045 Å for all van der Waals (vdW) interactions in the entire interface model and therefore analytical dispersion correction was not needed.

The polymer network and substrate interacted by the vdW force alone, which was modeled through the Lennard-Jones (LJ) potential. We replaced the optimized vdW parameters of carbon atoms in graphene used in Ref. 20 ($\epsilon = 0.3556$ kJ/mol and $\sigma = 3.67$ Å) with the actual parameters for carbon atoms in graphite which are used in this work, for the purpose of comparing the effect of graphite and silica substrates. The vdW parameters of silica and graphite atoms are given in Table II. The ϵ and σ values opted in this work for Si and O are capable of reproducing the real wettability of the silica surface without attaching hydroxyl groups.³⁰ The parameters for cross interactions between different atom types were determined using Lorentz-Berthelot mixing rules.

III. SIMULATION METHOD

All simulations in this work are carried out using the LAMMPS (Large-scale Atomic/Molecular Massively

Parallel Simulator) code for MD simulations.³¹ The interface separation simulation strategy used in this work closely follows the method in Ref. 20. The size of silica and graphite substrates was chosen to be the same for effective comparison. The polymer network in both GSI and SSI contained 80 *cis*-1,4-PI chains each having 24 monomers. This size was determined after conducting several simulations, with various chain lengths and total number of chains to obtain the $\tau - \delta$ plot in Ref. 20. It was seen that the system containing 80 chains, each having a length of 24 monomers, was the smallest network which produced the qualitatively converged $\tau - \delta$ plot. Please refer the equilibrated SSI and GSI shown in Fig. 1 to better understand the interface structure. In order to create the silica substrate for the interface, a slab of thickness (z direction) 5×3.348 Å ($= 16.74$ Å) and widths (xy -plane) matching the polymer network was carved out from the bulk amorphized silica. The value 3.348 Å is the interplanar distance between graphene layers in the graphite substrate, and it is multiplied with 5 since 6 layers of graphene were used. The widths of the substrates were approximately 60 Å, but there was a slight difference between the widths of graphite and silica substrates which is negligible and has no effect on the qualitative comparisons made in this article. This difference arises because the width of the graphite was a multiple of its unit cell dimension and the value of width was decided such that the width of the nanoplatelet will not exceed that of the polymer network.

The periodic box of the polymer network was unwrapped in the z -direction and the substrate was placed at one end, in the xy -plane. The interfaces generated from silica and graphite were equilibrated under isothermal-isobaric [NPT - fixed number of particles (N), a fixed pressure (P) and a fixed temperature (T)] ensemble for 510 ps at 1 atm pressure and at temperature at which the interface separation has to be conducted later. All MD simulations of interfaces

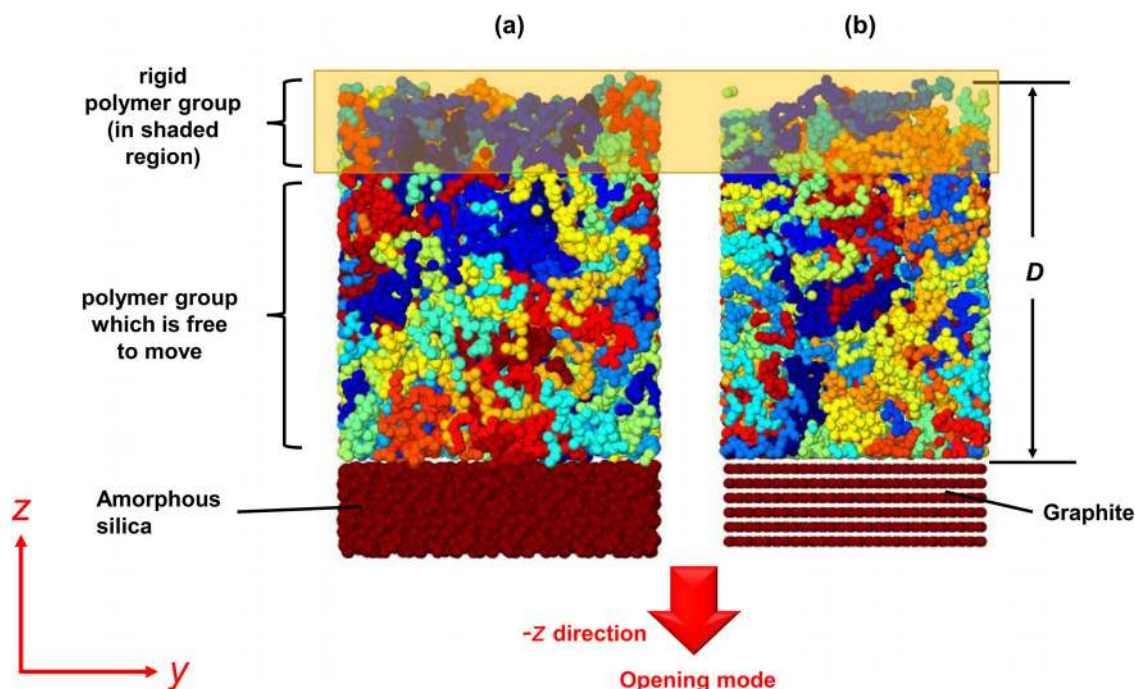


FIG. 1. Interfaces prepared for separation simulations: (a) silica-*cis*-1,4-PI and (b) graphite-*cis*-1,4-PI. The direction of separation is marked with a red arrow.

were carried out with a timestep of 0.3 fs and all NPT ensembles generated were at 1 atm pressure. The equilibration of the interface was identified by the convergence of cohesive binding energy of the interface. The top part of the polymer network (marked with a box shaded in yellow in Fig. 1) was kept fixed during interface separation. The thickness of the fixed polymer layer is $(2/7)D$, where D is the thickness of the polymer network after interface equilibration. The substrates were kept rigid during all MD simulations. The area of the substrate projected on the xy -plane was used to estimate the traction resulting from the interface force interactions.

In the present work, the SSI and the GSI are compared based on the normal traction (τ_n) experienced on the substrate while the interface separates (δ_n) in the opening mode at various rates and temperatures. The range of separation rates opted in this work are exhaustive enough to contain various phenomena observed in Ref. 20. The effect of separation rate is detailed in Sec. IV prior to the discussion of the results. The separation rates employed include quasistatic separation and various finite rates. In order to simulate the quasistatic separation, the substrate was moved in steps of 0.25 \AA while the polymer excluding the fixed part underwent dynamics which sampled microcanonical [NVE - fixed number of particles (N), a fixed volume (V) and a fixed energy (E)] ensemble. The mobile polymer was minimized subsequently keeping the substrate intact. The mobile polymer was then equilibrated in the NPT ensemble for 30 ps while the substrate remains immobile. An ensemble average of traction was taken at each separation step. The step-wise separation was replaced with a continuous separation in order to simulate finite rates. The substrate moved at a uniform finite separation rate when the mobile polymer atoms undergo NPT dynamics. The traction was recorded continuously as the interface separated. Temperatures of 305 K and 410 K were chosen in order to understand how temperature affects the traction response. 305 K is chosen since it is a representative of the ambient room temperature whereas 410 K was opted because the *cis*-1,4-PI is fully melt at this temperature.³² The T_g of the bulk *cis*-1,4-PI network used in this work determined using MD simulation is 304.2 K.²⁰ Hence the temperatures used in this study are above the T_g of polymer matrix. All separation simulations were conducted at 305 K except those which were intended to study the effect of temperature.

A. Analysis tools

In order to assess the effect of the presence of either substrates on the polymer and to justify several claims made throughout this article, various static and dynamic properties of the unseparated interface configuration were needed. The computation of those properties and various other measures used in this article to analyze the separation behavior are detailed below.

1. Density (ρ): to understand the packing of the polymer over each substrate (graphite or silica), the density distribution of the polymer was determined. The polymer region was subdivided into slabs of 0.5 \AA thickness and the density of each slab was determined. The density of each slab was then averaged over time in the NPT

ensemble and the standard deviation was used as a measure of the error. The density was then plotted as a function of distance (r_{slab}) from the center of the slab closest to the substrate. One of the concerns which arose while comparing the density distributions (between GSI and SSI) is that the error bars were large for slab thickness as low as 0.5 \AA . This resulted in the error bars overlapping for distances far from the interface (large r_{slab}) making it difficult to conclude on the effect of substrate on the bulk density at these distances. In order to check whether the qualitative comparison provided by the means was a reliable indicator of the density, a larger slab thickness of 5 \AA was also used. Furthermore, the mean density of a region of thickness 19 \AA (ρ_{int}), whose base is 1.5 \AA above the interface was calculated to see how far the effect of the interphase penetrated into the bulk material.

2. The mean square displacement (MSD) of the polymer in GSI and SSI with respect to time was obtained after the interface equilibration was achieved. MSD was calculated for all polymer atoms as $\text{MSD}(t) = \langle |\mathbf{r}(t) - \mathbf{r}(0)|^2 \rangle$, where $\mathbf{r}(t)$ is the position at time t and $\mathbf{r}(0)$ is the reference position of each atom. The squared displacement corresponding to each atom is averaged for the entire system at each timestep to obtain the MSD at that time. The slope of the straight line that fits the MSD curve (m_{MSD}) was taken as the quantification for the mobility of polymer in the corresponding interface.
3. The vdW ($U_{\text{vdW.poly}}$), bond (U_{bond}), angle (U_{angle}), and dihedral (U_{dihed}) interaction energies within the polymer were determined to understand the effect of substrates on the polymer.
4. Stiffness of the polymer (K_p): to determine the role of the substrate on the tendency of the polymer network to resist deformation, the stiffness of the polymer was computed. This quantity was obtained from the plot of volume average of normal stress in the z direction within the polymer with respect to the strain of the simulation box. The volume average of stress was calculated using the “compute stress/atom” function of LAMMPS and the voronoi volume of each atom was calculated using the code written by Chris Rycroft.³³ The stress/atom quantity returns virial stress for each atom. The slope of the initial linear elastic region of this plot quantifies K_p when the interface undergoes uniaxial tension in the z -direction keeping the simulation box volume constant. The strain rate for uniaxial tension was $1.2983 \times 10^{-7} \text{ fs}^{-1}$, which was obtained by dividing the equivalent finite separation rate ($8.33 \times 10^{-6} \text{ \AA/fs}$) corresponding to the quasistatic separation with the thickness of the polymer network. The equivalent finite rate was obtained by dividing the separation step ($= 0.25 \text{ \AA}$) with the NPT equilibration time at each separation step ($= 30 \text{ ps}$).
5. Entanglement strength of the polymer (K_{ent}): this is a measure of locking of the polymer chains due to their proximity to other chains. It was calculated as the sum of local periodic linking number (LK) corresponding to each chain in the network. LK was derived using the Gauss linking number.³⁴ The proximity of neighboring chains has a significant contribution to the LK which is

computed for a chain, even though a complete intertwining of chains may not exist. It is proved that LK produces the entanglement strength estimate same as the CReTa³⁵ and Z1³⁶ algorithms which are commonly used to quantify the entanglements in the polymer network.³⁴

6. Strength modulus (K_τ): this parameter quantifies the strength of the interface and is defined as the ratio of the peak traction (τ_p) to the separation at the peak traction.
7. Work of adhesion (W_{adh}): area under the $\tau_n - \delta_n$ plot.
8. Bound polymer: amount of chains adhered to the substrate after fracture. It is expressed as the percentage of adhered chains out of the total number of chains in the interface.
9. It was found in Ref. 20 that the $\tau_n - \delta_n$ plot had a very close correlation with the evolution of voids during separation. For this reason, the $\tau_n - \delta_n$ plot is accompanied by plots depicting the evolution of voids. To define these voids, the domain was divided into several cubic cells (5 Å size). Empty cells were clustered using the Hoshen-Kopelman algorithm.³⁷ Each empty cell was termed a “void” and an empty region with a minimum of 3 voids was a “void cluster”. The evolution of the quantities, number of void clusters and the size of the largest void cluster, during separation, provide insights into mechanisms taking place during the separation.
10. To quantify chain straightening, the projection of the contour of the chain (which straightened most during separation) on the direction normal to the plane of the substrate (that is, the z -direction) was used.

IV. CERTAIN FEATURES OF COHESIVE FILLER-POLYMER INTERFACE SEPARATION

Understanding certain phenomena observed during the opening mode separation of the graphene-*cis*-1,4-PI cohesive interface mentioned in Ref. 20 is required to interpret and explain the results of this work. These phenomena are recapitulated here.

1. In the softening region of the quasistatic traction response at low temperatures (~ 305 K), there existed a region where the traction was almost constant. This region is termed as the *plateau*. This plateau was shown to be a result of generation and annihilation of void clusters (at equal rates) in the bridging phase of separation, preceding fracture. This process occurs due to the availability of a large space in the interface region. The plateau is characterized by the large mobility of chains in the bridging zone. Significant fluctuations were observed in the size of the largest void cluster corresponding to the plateau region.
2. The separation rate significantly affects the mechanical behavior of the interface. Depending on the interface response, the separation rates can be categorized as quasistatic, intermediate, and rapid. The characteristic features of these categories are as follows.
 - *Quasistatic*: the interface is always in mechanical equilibrium during separation. This aspect provides the chains sufficient time to comfortably disentangle and respond to the applied load. If the interface cohesion is sufficiently high (as it was in Ref. 20), voids develop

within the polymer network resulting in the failure of the polymer with a significant amount of bound polymer on the substrate. Such a behavior is also applicable for lower values of finite separation rates for which the traction response and the deformation physics are qualitatively similar to quasistatic separation.

- *Intermediate rates*: the interface is not in mechanical equilibrium during separation. These rates are sufficiently large such that the timescale of polymer atom vibration is comparable with that of the substrate separation. The frequency of atomic vibration is $\sim 10^{13}$ Hz where atoms can be assumed to be connected by springs whose length is equal to the mean bond length ($= 1.48$ Å). Calculation based on these values renders the order of the mean vibrational velocity of atoms to be $\sim 10^{-3}$ Å/fs which is the same as the order of intermediate rates. Due to the resultant comparable timescales, the polymer chains do not have sufficient time to disentangle themselves completely and this results in the massive straightening of chains, as the interface is separated. The inertia of the chains to the separation also resulted in a jerk at the substrate due to the interface cohesive binding causing, a large pulse of traction at the onset of separation. At intermediate rates, the amount of bound polymer reduces as the magnitude of rate increases.
- *Rapid rates*: at very high rates, the interface deformation resembles two separating rigid bodies (polymer and substrate, here) with negligible dynamics of the polymer in the timescales of separation. There is no bound polymer and the fracture happens at the interface.

V. RESULTS AND DISCUSSION

A. Role of substrate

Table III summarizes the properties of unseparated GSI and SSI. Clearly, the differences arising between these two configurations are only due to the substrate, since the polymer material is exactly same. Below, each of these properties is examined carefully.

Figure 2(a) shows the density profiles of SSI and GSI as a function of the distance from the interface. The profile of GSI exhibits a higher peak (2.69 g/cm³) than SSI (1.66 g/cm³) which indicates a denser interphase for GSI. The dense

TABLE III. Comparison of various properties for the unseparated GSI and SSI at 305 K.

Interface type → Property ↓	SSI	GSI
ρ_{bulk} (g/cm ³)	0.81 ± 0.14	0.74 ± 0.14
ρ_{int} (g/cm ³)	0.79 ± 0.01	0.74 ± 0.01
E_{coh} (kJ/mol)	-3148.42 ± 61.80	-6853.64 ± 93.89
m_{MSD} (Å ² /ps)	0.52	1.10
$U_{\text{vdW, poly}}$ ($\times 10^2$ kJ/mol)	-384.79 ± 2.51	-347.67 ± 3.22
U_{bond} ($\times 10^2$ kJ/mol)	176.84 ± 2.53	233.11 ± 3.28
U_{angle} ($\times 10^2$ kJ/mol)	177.30 ± 2.56	229.96 ± 3.35
U_{dihed} ($\times 10^2$ kJ/mol)	-181.35 ± 1.46	-164.94 ± 1.88
K_p (kJ/mol·Å ³)	17.82	15.40
K_{ent}	2.7878 ± 0.6763	1.2789 ± 0.4953

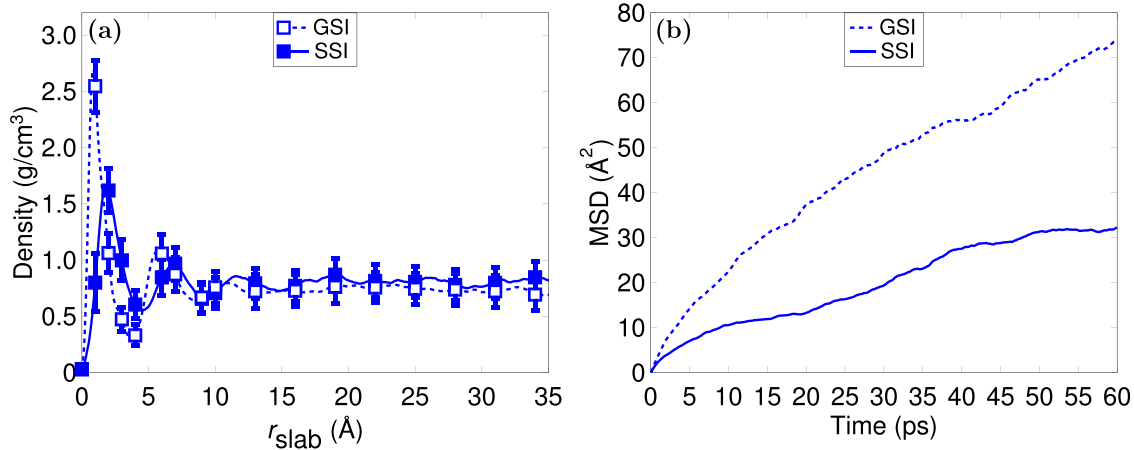


FIG. 2. (a) The density profile of the polymer network in SSI and GSI as a function of the distance from the interface. (b) Mean square displacement of polymer atoms with respect to time at 305 K.

interphase in GSI is a result of higher interface binding which is twice as strong as that in SSI, as indicated by the interface cohesive energy (E_{coh}) in Table III. Despite the dense interphase, the mean of the densities corresponding to slabs far from the interface [large r_{slab} in Fig. 2(a)] is slightly lower for GSI than SSI (Table III). This density (far from the interface) is termed as bulk density (ρ_{bulk}) in this paper. The ρ_{bulk} were 0.81 ± 0.14 and 0.74 ± 0.14 g/cm³, respectively, for SSI and GSI corresponding to a 0.5 \AA thick slab, while 0.80 ± 0.03 and 0.74 ± 0.03 g/cm³, respectively, when slabs of 5 \AA thickness were used. Although there was a difference in the ρ_{bulk} value for SSI and GSI, the densities were quite close to 0.83 g/cm^3 which is the density of a periodic bulk system of *cis*-1,4-PI with mean chain length 24 monomers.²⁰ Since, the density differences are not significant enough to draw conclusions concerning the variations in the behavior of the interfaces, other properties have to be considered. Furthermore, ρ_{int} was found to be larger for SSI (Table III) which indicates that the effect of interphase density had vanished much before $r_{\text{slab}} = 21.0 \text{ \AA}$. It can be concluded therefore that the interphase was confined to the interface ($r_{\text{slab}} < 21.0 \text{ \AA}$) and it did not penetrate far into the polymer.

Figure 2(b) shows the plot of the MSD of polymer atoms in GSI and SSI with respect to time. The curve corresponding to polymer in GSI is clearly above the one corresponding

to the SSI. m_{MSD} are 1.10 and $0.52 \text{ \AA}^2/\text{ps}$, respectively, for GSI and SSI (Table III) indicating that the polymer above graphite is more mobile. Further, $U_{\text{vdW, poly}}$, U_{bond} , U_{angle} , and U_{dihed} are lower in the case of SSI which means that the polymer in SSI is energetically more stable than that in GSI (Table III).

The K_p in SSI was found to be larger than GSI (Table III). The K_{ent} is also estimated to be larger for the polymer in SSI than in GSI (Table III). The stiffness and entanglement quantifications obtained indicate that it is difficult to separate the polymer in SSI into two sections by pulling it in a direction normal to the substrate surface. Significant differences observed for E_{coh} , m_{MSD} , potential energy of the polymer, K_p and K_{ent} prove the effect of the substrate on the static and dynamic properties of GSI and SSI.

B. Quasistatic opening mode of separation

The $\tau_n - \delta_n$ characteristics and the void features of both GSI and SSI, when they were separated quasistatically at 305 K, are shown in Fig. 3. The interface strength parameters (τ_p , K_τ , and W_{adh}) of GSI and SSI at various rates measured at 305 K are presented as cartoon plots in Fig. 4. It is observed that SSI has a higher τ_p at smaller separation resulting in larger K_τ when compared to GSI. The W_{adh} ,

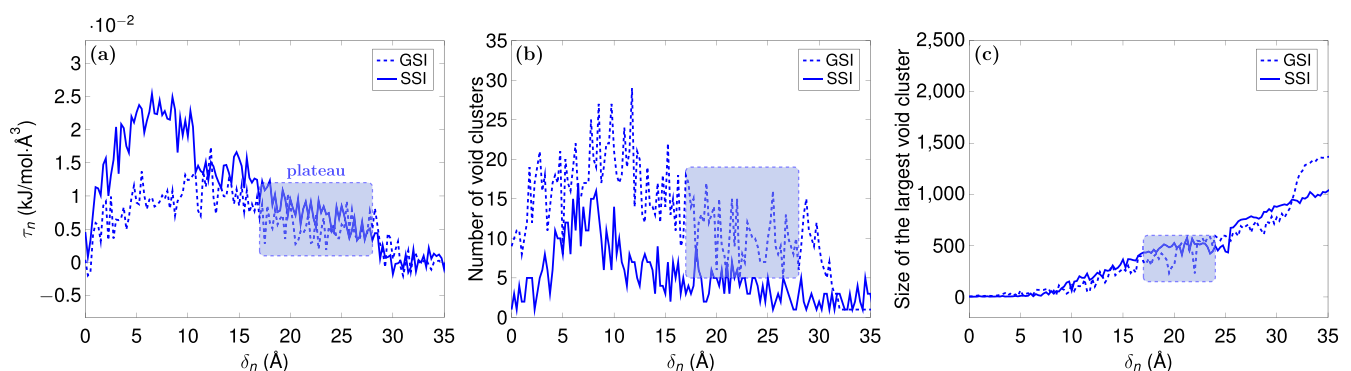


FIG. 3. Traction response and the associated void evolution in quasistatic opening mode separation at 305 K. (a) $\tau_n - \delta_n$ plot, (b) variation of number of void clusters with separation, and (c) variation of size of the largest void cluster. The region of the plot that contains salient features of the plateau phenomenon is marked in all subfigures.

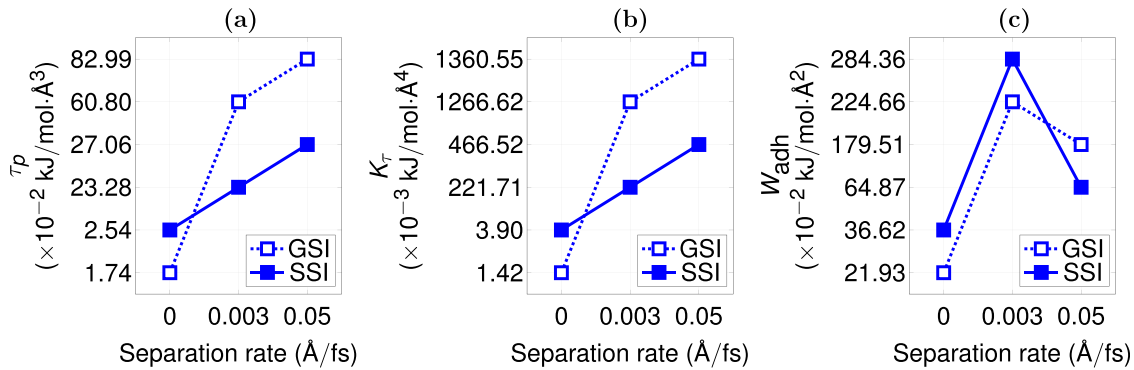


FIG. 4. Representation of the dependence of the interface strength parameters - (a) τ_p , (b) K_τ , and (c) W_{adh} - of GSI and SSI on the separation rate at 305 K. The separation rate 0 Å/fs represents quasistatic separation.

which is the energy required to separate an interface, is also higher for SSI than GSI. However, following the separation, the amount of bound polymer on both graphite and silica is 31.25% of the total number of chains. The large amount of bound rubber indicates that the fracture happened within the polymer bulk. A plateau region is noticeable during the traction decay in GSI from $\delta_n=17$ Å to 28 Å which is marked in Fig. 3(a). No significant plateau was observed in SSI. The presence of a plateau in the GSI is corroborated by significant fluctuations in the size of the largest void cluster [Fig. 3(c)]. The evolution of void clusters [Fig. 3(b)] in both SSI and GSI maintains complete correlation with their respective traction responses [Fig. 3(a)]. However, the number of void clusters is always less in SSI than GSI, but the size of the largest void cluster is nearly the same in both SSI and GSI [Fig. 3(c)].

The three factors representing the interface strength (τ_p , K_τ , W_{adh}) were (0.83×10^{-2} kJ/mol·Å³, 0.49×10^{-3} kJ/mol·Å⁴, and 6.34×10^{-2} kJ/mol·Å²) for GSI and (1.52×10^{-2} kJ/mol·Å³, 1.15×10^{-3} kJ/mol·Å⁴, 21.28×10^{-2} kJ/mol·Å²) for SSI at 410 K. Both GSI and SSI indicate lower interface strength at 410 K compared to 305 K (refer Fig. 4), which is characterized by the delayed lower magnitude of τ_p during separation at 410 K. The lower strength of the interface at 410 K is the result of softening of the polymer which is expected with the temperature rise, since the mobility of the polymer atoms increases with temperature. SSI is stronger than GSI at both 305 K and 410 K as indicated by τ_p , K_τ , and W_{adh} . The amount of bound polymer was nearly the same in GSI and SSI at 410 K (31.25% and 28.75%, respectively) which is the same as the amount of bound polymer at 305 K.

The higher strength exhibited by SSI in quasistatic separation can be understood based on the discussion made in Sec. V A. It was shown that the binding of the polymer with silica is weaker when compared with graphite, as indicated by the corresponding E_{coh} values (Table III). In spite of this, SSI seems to have a higher strength. To explain this, we note that at quasistatic rates of separation, there is sufficient time for the chains to disentangle themselves and react to the applied separation. At such low rates, the failure is dominated by what happens at the bulk of the polymer and not the interface.²⁰ The higher stiffness, entanglement strength, lower potential energy, and lower mobility of the polymer in SSI result in larger strength of the polymer material over the

silica and hence SSI has higher strength. Furthermore, the slightly large bulk polymer density and lower polymer potential energy indicates that the polymer over silica is more compact than that over graphite. This aspect makes it difficult to disentangle the chains in polymer over silica due to which the generation of voids also becomes difficult. Higher bulk density and stability of the polymer are also the reasons for the fewer number of void clusters in SSI during quasistatic separation. The lower mobility of the polymer dampens the chain dynamics during the bridging phase thereby making the plateau insignificant during the quasistatic traction response of SSI.

C. Interface separation in the opening mode at finite rates

Figures 5(a) and 5(b) show the $\tau_n - \delta_n$ characteristics of SSI and GSI at the intermediate and rapid rates, respectively. Separation rates of 3×10^{-3} Å/fs and 5×10^{-2} Å/fs imparted the intermediate and rapid rate responses, respectively, for both GSI and SSI. The inertia driven τ_p at the intermediate and rapid rates is one order higher than the quasistatic τ_p . The strength parameters of the traction response are presented in Fig. 4. It is observed that GSI has higher τ_p and K_τ at both intermediate and rapid rates. SSI has a slightly higher W_{adh} than GSI at the intermediate rate, but the values are comparable. The W_{adh} is higher for GSI than SSI at the rapid rate. The amount of bound polymers in GSI and SSI at the rate 3×10^{-3} Å/fs were 22.5% and 16.25%, respectively. The bound polymer reduced as the rate increased from quasistatic to rapid, with absolutely no bound polymer at the rapid rate. This indicates that the fracture position shifted from the polymer bulk to the interface as the rate was increased from quasistatic to rapid rate.

As discussed in Sec. V A, the GSI has larger cohesive energy and this results in a large inertial force and consequently a higher τ_p and K_τ when compared to SSI at intermediate and rapid rates. As the stiffness of the polymer network increases, more energy is needed to straighten and shear the chains past each other. W_{adh} at intermediate rates is the sum of the energies required to overcome the τ_p and to deform the chains. Therefore, the higher cohesive energy of the interface in GSI and the stiff polymer in SSI are competing factors to decide which the interface has more W_{adh} . SSI

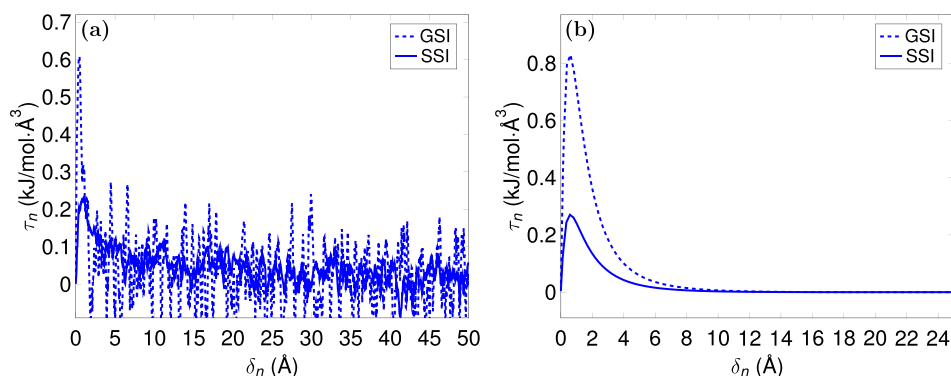


FIG. 5. Traction response in the opening mode of separation at 305 K for the separation rates, (a) $3.0 \times 10^{-3} \text{ \AA/fs}$ and (b) $5.0 \times 10^{-2} \text{ \AA/fs}$.

($2.84 \text{ kJ/mol}\cdot\text{\AA}^2$) dominates with slightly more W_{adh} than GSI ($2.25 \text{ kJ/mol}\cdot\text{\AA}^2$) though the values are quite close. At rapid rates, the interface cohesive energy is the only deciding factor as there is no chain deformation and hence the W_{adh} was higher for GSI. The values of W_{adh} required to separate GSI and SSI were the highest at the intermediate separation rate [Fig. 4(c)] since the substrate has to provide energy to overcome both interface cohesion and to deform the polymer network. It can be concluded that the interface cohesive energy was the decisive factor which imparted greater strength to GSI than SSI at intermediate and rapid rates.

The evolution of voids and chain straightening with respect to separation at the intermediate rate are shown in Fig. 6. The peak number of void clusters is higher in the GSI [Fig. 6(a)] since the polymer it contains has lower stiffness, lower bulk density, and higher mobility (compared to the polymer in SSI) due to which it is easier to generate voids. After the peak, the number of void clusters was almost equal

in both GSI and SSI. The size of the largest void cluster was almost the same in both GSI and SSI [Fig. 6(b)]. It is observed that the straightening of the chains in GSI is more than that in SSI [Fig. 6(c)], since the high interface cohesive energy in GSI pulls the chain along with the other favorable factors like lower bulk density, higher mobility and lower polymer stiffness.

In order to further explore the consequences due to different static and dynamic properties of GSI and SSI, the interfaces were separated at $7 \times 10^{-3} \text{ \AA/fs}$ which is between the intermediate and rapid rates discussed above ($3 \times 10^{-3} \text{ \AA/fs}$ and $5 \times 10^{-2} \text{ \AA/fs}$, respectively). It was interesting to observe that GSI produced an intermediate rate traction response whereas SSI produced traction response depicting a rapid rate [Fig. 7(a)]. The number of void clusters in SSI was less and nearly constant during the separation which indicates negligible chain deformation [Fig. 7(b)]. The visuals of interface separation of GSI and SSI at the separation rate

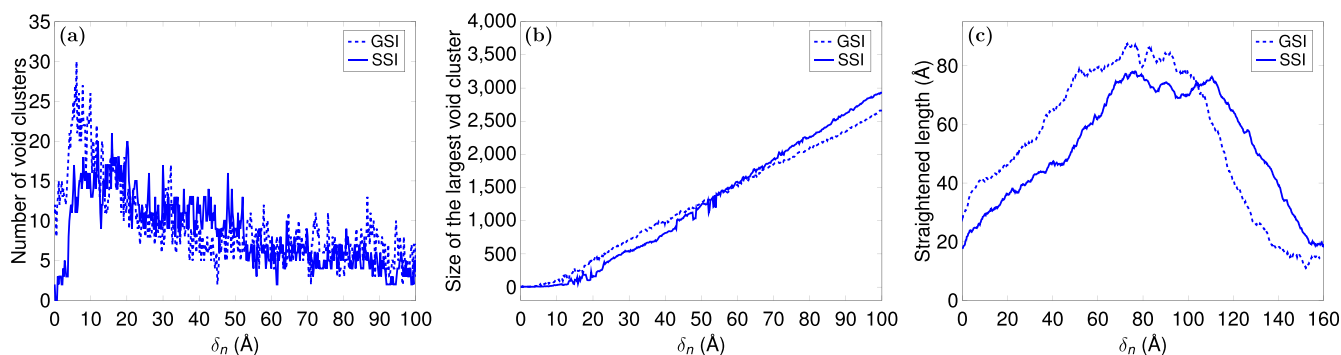


FIG. 6. Void development and chain straightening in the interfaces during the opening mode of separation at 305 K at the rate $3.0 \times 10^{-3} \text{ \AA/fs}$. (a) Evolution of void clusters, (b) variation of size of the largest void cluster, and (c) chain straightening, plotted against separation.

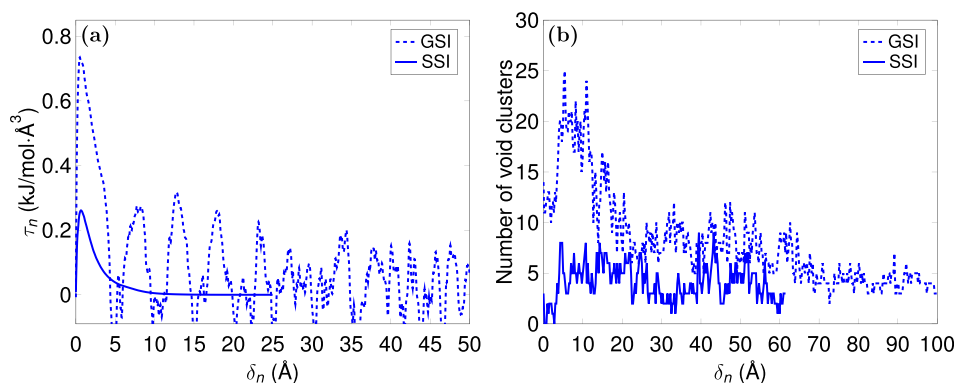


FIG. 7. Traction response and the evolution of void clusters in opening mode separation at 305 K for the separation rate $7.0 \times 10^{-3} \text{ \AA/fs}$. (a) $\tau_n - \delta_n$ plot and (b) the evolution of void clusters.

$7 \times 10^{-3} \text{ \AA/fs}$ are presented in a video as [supplementary material](#). The biased perception of the separation rate happens due to the tendency of the polymer above silica to act as a rigid body due to its high stiffness. The strength parameters, viz., τ_p , K_τ and W_{adh} are higher for GSI ($73.48 \times 10^{-2} \text{ kJ/mol} \cdot \text{ \AA}^3$, $1469.59 \times 10^{-3} \text{ kJ/mol} \cdot \text{ \AA}^4$, and $549.67 \times 10^{-2} \text{ kJ/mol} \cdot \text{ \AA}^2$) than SSI ($26.11 \times 10^{-2} \text{ kJ/mol} \cdot \text{ \AA}^3$, $395.64 \times 10^{-3} \text{ kJ/mol} \cdot \text{ \AA}^4$, and $75.67 \times 10^{-2} \text{ kJ/mol} \cdot \text{ \AA}^2$) at $7 \times 10^{-3} \text{ \AA/fs}$ separation rate. At this rate, the W_{adh} is the energy only to overcome the interface cohesive energy in the case of SSI whereas for GSI, it also involves the energy associated with chain deformation. The bound polymer in GSI was 16.25% whereas no bound polymer was present in SSI as it produced rapid rate response.

VI. CONCLUSIONS

This work focused on comparing the interface strength of the amorphous silica-*cis*-1,4-PI interface and graphite-*cis*-1,4-PI interface using the opening mode $\tau - \delta$ characteristics. The interface separations were simulated at quasistatic, intermediate, and rapid rates. This categorization of the separation rates is exhaustive to include all types of interface responses to substrate separation in a cohesive interface at all temperatures.²⁰ The effect of temperature (above T_g) on quasistatic separation was also studied.

In order to explore the effect of substrate on interface traction response and deformation physics, various static and dynamic properties of GSI and SSI were determined at 305 K. GSI had better binding due to larger interface cohesive energy than SSI. The polymer in SSI was energetically more stabler, with lower chain mobility and slightly larger bulk polymer density than what was observed for GSI. Moreover, the polymer in SSI was stiffer and it had more entanglement strength than the polymer in GSI. The observation that, the separation rate $7 \times 10^{-3} \text{ \AA/fs}$ was a rapid rate for SSI while it was an intermediate rate for GSI at 305 K, shows that the polymer over SSI is stiffer.

At quasistatic separation (305 K temperature), SSI had larger strength parameters, viz., peak traction (τ_p), strength modulus (K_τ), and work of adhesion (W_{adh}) as compared to GSI. Higher strength of SSI at quasistatic separation is supported by the better stability and higher values of stiffness and entanglement strength of the polymer contained in it, since the fracture happens within the polymer bulk when the interface separates quasistatically. When the temperature was increased to 410 K, the larger thermally induced mobility of polymer atoms made the interface *softer*, which brought down the strength of both SSI and GSI. However, SSI maintained its higher strength over GSI. The higher strength of SSI over GSI will persist at lower values of finite separation rates as well since the separation behavior at these rates is similar to the quasistatic separation.

As the separation rates were increased, we observed a cross-over in the interface strength, which shifted to GSI from SSI (refer Fig. 4). At intermediate and rapid rates, the τ_p and K_τ were higher for GSI due to the larger interface cohesion in GSI compared to SSI. The W_{adh} was comparable for both interfaces in the intermediate rate with SSI having a slightly higher value, but the W_{adh} was clearly higher for GSI

at the rapid rate. This is because the W_{adh} at the intermediate rate includes the energy to deform the polymer chains also, which is higher for the polymer in SSI, in addition to the energy required to overcome the interface cohesion which is involved in both intermediate and rapid rates.

The interface deformation during separation was examined based on the void development and chain straightening. It was observed that the deformation physics qualitatively agrees with each other in GSI and SSI and is in accordance with the interface deformation physics discussed in Ref. 20. The quantitative difference in void development and chain straightening between both interface types is explained using the static and dynamic properties of the unseparated GSI and SSI. The amount of bound polymer reduced in both types of interfaces as the separation rate increased and there was no bound polymer after separation in the rapid rate. This implies that the fracture happened in the polymer bulk during quasistatic separation, but it shifted towards the interface as the rate increased. The slightly rapid reduction of the quantity of the bound polymer in SSI with respect to the increase in the separation rate, as compared to GSI, is due to the stiffer polymer network in SSI.

The equivalent finite rate for the quasistatic separation in this work is 0.83 m/s ($= 8.33 \times 10^{-6} \text{ \AA/fs}$). The local strain rates in an automobile tire tread material are very unlikely to go up to this level. Therefore, silica fillers are more suitable than carbon black fillers for imparting better interface strength in automobile tire material resulting in the reduction of rolling resistance. However, carbon black fillers are suitable when the rubber nanocomposite has to withstand large impact loads where the rates are very high.

SUPPLEMENTARY MATERIAL

See [supplementary material](#) for interface separation visuals of GSI and SSI at the rate of $7 \times 10^{-3} \text{ \AA/fs}$, which is presented in the video interface_effect.avi.

ACKNOWLEDGMENTS

We acknowledge the computing facilities from the P. G. Senapathy Center for Computing Resource at IIT Madras.

¹J. T. Byers, "Fillers for balancing passenger tire tread properties," *Rubber Chem. Technol.* **75**, 527–548 (2002).

²A. Hilonga, J. K. Kim, P. B. Sarawade, D. V. Quang, G. N. Shao, G. Elineema, and H. T. Kim, "Synthesis of mesoporous silica with superior properties suitable for green tire," *J. Ind. Eng. Chem.* **18**, 1841–1844 (2012).

³S. S. Choi, "Filler-polymer interactions in both silica and carbon black-filled styrene-butadiene rubber compounds," *J. Polym. Sci., Part B: Polym. Phys.* **39**, 439–445 (2001).

⁴M. J. Wang, S. X. Lu, and K. Mahmud, "Carbon-silica dual-phase filler, a new-generation reinforcing agent for rubber. part vi. time-temperature superposition of dynamic properties of carbon-silica-dual-phase-filler-filled vulcanizates," *J. Polym. Sci., Part B: Polym. Phys.* **38**, 1240–1249 (2000).

⁵M. Rahmat and P. Hubert, "Carbon nanotube-polymer interactions in nanocomposites: A review," *Compos. Sci. Technol.* **72**, 72–84 (2011).

⁶Z. Yang, J. Liu, R. Liao, G. Yang, X. Wu, Z. Tang, B. Guo, L. Zhang, Y. Ma, Q. Nie, and F. Wang, "Rational design of covalent interfaces for graphene/elastomer nanocomposites," *Compos. Sci. Technol.* **132**, 68–75 (2016).

- ⁷J. R. Potts, O. Shankar, S. Murali, L. Du, and R. S. Ruoff, "Latex and two-roll mill processing of thermally-exfoliated graphite oxide/natural rubber nanocomposites," *Compos. Sci. Technol.* **74**, 166–172 (2013).
- ⁸N. Yousefi, M. M. Gudarzi, Q. Zheng, X. Lin, X. Shen, J. Jia, F. Sharif, and J. K. Kim, "Highly aligned, ultralarge-size reduced graphene oxide/polyurethane nanocomposites: Mechanical properties and moisture permeability," *Composites, Part A* **49**, 42–50 (2013).
- ⁹A. P. Awasthi, D. C. Lagoudas, and D. C. Hammerand, "Modeling of graphene-polymer interfacial mechanical behavior using molecular dynamics," *Modell. Simul. Mater. Sci. Eng.* **17**, 015002 (2009).
- ¹⁰S. Lee, J. Park, J. Yang, and W. Lu, "Molecular dynamics simulations of the traction-separation response at the interface between pvdf binder and graphite in the electrode of li-ion batteries," *J. Electrochem. Soc.* **161**, A1218–A1223 (2014).
- ¹¹Y. Zhang, X. Zhuang, J. Muthu, T. Mabrouki, M. Fontaine, Y. Gong, and T. Rabczuk, "Load transfer of graphene/carbon nanotube/polyethylene hybrid nanocomposite by molecular dynamics simulation," *Composites, Part B* **63**, 27–33 (2014).
- ¹²M. P. Manoharan, A. Sharma, A. V. Desai, M. A. Haque, C. E. Bakis, and K. W. Wang, "The interfacial strength of carbon nanofiber epoxy composite using single fiber pullout experiments," *Nanotechnology* **20**, 295701 (2009).
- ¹³Y. Li and G. D. Seidel, "Multiscale modeling of functionalized interface effects on the effective elastic material properties of cnt-polyethylene nanocomposites," *Comput. Mater. Sci.* **107**, 216–234 (2015).
- ¹⁴R. Rahman and A. Haque, "Molecular modeling of crosslinked graphene-epoxy nanocomposites for characterization of elastic constants and interfacial properties," *Composites, Part B* **54**, 353–364 (2013).
- ¹⁵R. Rahman, J. T. Foster, and A. Haque, "Molecular dynamics simulation and characterization of graphene-cellulose nanocomposites," *J. Phys. Chem. A* **117**, 5344–5353 (2013).
- ¹⁶M. Solar, Z. Qin, and M. J. Buehler, "Molecular mechanics and performance of crosslinked amorphous polymer adhesives," *J. Mater. Res.* **29**, 1077–1085 (2014).
- ¹⁷W. Xia and S. Keten, "Coupled effects of substrate adhesion and intermolecular forces on polymer thin film glass-transition behavior," *Langmuir* **29**, 12730–12736 (2013).
- ¹⁸Y. Hu and J. Ding, "Effects of morphologies of carbon nanofillers on the interfacial and deformation behavior of polymer nanocomposites—A molecular dynamics study," *Carbon* **107**, 510–524 (2016).
- ¹⁹Z. Yuan, Z. Lu, Z. Yang, J. Sun, and F. Xie, "A criterion for the normal properties of graphene/polymer interface," *Comput. Mater. Sci.* **120**, 13–20 (2016).
- ²⁰J. Jose, B. V. T., and N. Swaminathan, "Insights into traction-separation phenomena of graphene-cis-1,4-polyisoprene interface using molecular dynamics," *Polymer* **122**, 280–295 (2017).
- ²¹J. S. Kulesh and L. Pauling, "The problem of the graphite structure," *Am. Mineral.* **35**, 125 (1950); available at http://www.minsocam.org/msa/collectors_corner/amtoc/toc1950.htm.
- ²²S. Dong, J. Yan, N. Xu, J. Xu, and H. Wang, "Molecular dynamics simulation on surface modification of carbon black with polyvinyl alcohol," *Surf. Sci.* **605**, 868–874 (2011).
- ²³S. J. Stuart, A. B. Tutein, and J. A. Harrison, "A reactive potential for hydrocarbons with intermolecular interactions," *J. Chem. Phys.* **112**, 6472–6486 (2000).
- ²⁴T. F. W. Barth, "The cristobalite structures," *Am. J. Sci. Ser. 5* **23**, 350–356 (1932).
- ²⁵R. G. D. Valle and H. C. Andersen, "Molecular dynamics simulation of silica liquid and glass," *J. Chem. Phys.* **97**, 2682–2689 (1992).
- ²⁶O. M. Roscioni, L. Muccioli, R. G. Della Valle, A. Pizzirusso, M. Ricci, and C. Zannoni, "Predicting the anchoring of liquid crystals at a solid surface: 5-cyanobiphenyl on cristobalite and glassy silica surfaces of increasing roughness," *Langmuir* **29**, 8950–8958 (2013).
- ²⁷J. Du and A. N. Cormack, "Molecular dynamics simulation of the structure and hydroxylation of silica glass surfaces," *J. Am. Ceram. Soc.* **88**, 2532–2539 (2005).
- ²⁸S. Tsuneyuki, M. Tsukada, H. Aoki, and Y. Matsui, "First-principles interatomic potential of silica applied to molecular dynamics," *Phys. Rev. Lett.* **61**, 869–872 (1988).
- ²⁹D. Curco and C. Aleman, "Simulation of dense amorphous polymers by generating representative atomistic models," *J. Chem. Phys.* **119**, 2915–2922 (2003).
- ³⁰E. R. Cruz-Chu, A. Aksimentiev, and K. Schulten, "Water-silica force field for simulating nanodevices," *J. Phys. Chem. B* **110**, 21497–21508 (2006).
- ³¹S. Plimpton, "Fast parallel algorithms for short-range molecular dynamics," *J. Comput. Phys.* **117**, 1–19 (1995).
- ³²M. Doxastakis, V. G. Mavrantzas, and D. N. Theodorou, "Atomistic Monte Carlo simulation of cis-1,4 melts. I. Single temperature end-bridging Monte Carlo simulations," *J. Chem. Phys.* **115**, 11339–11351 (2001).
- ³³C. H. Rycroft, "Voro++: A three-dimensional voronoi cell library in c++," *Chaos* **19**, 041111 (2009).
- ³⁴E. Panagiotou, C. Tzoumanekas, S. Lambropoulou, K. C. Millett, and D. N. Theodorou, "A study of the entanglement in systems with periodic boundary conditions," *Prog. Theor. Phys. Suppl.* **191**, 172–181 (2011).
- ³⁵C. Tzoumanekas and D. N. Theodorou, "Topological analysis of linear polymer melts: A statistical approach," *Macromolecules* **39**, 4592–4604 (2006).
- ³⁶M. Kroger, "Shortest multiple disconnected path for the analysis of entanglements in two- and three-dimensional polymeric systems," *Comput. Phys. Commun.* **168**, 209–232 (2005).
- ³⁷A. Al-Futaisi and T. W. Patzek, "Extension of hoshen-kopelman algorithm to non-lattice environments," *Physica A* **321**, 665–678 (2003).